Journal of Applied Physics | ARTICLE | pubs.aip.org/aip/jap

Diamond-like carbon conversion surfaces for space applications

Cite as: J. Appl. Phys. **135**, 185301 (2024); doi: 10.1063/5.0203686
Submitted: 15 February 2024 · Accepted: 15 April 2024 ·
Published Online: 8 May 2024

Justyna M. Sokół,[1,a)] Jianliang Lin,[2] Stephen A. Fuselier,[1,3] Travis Eliason,[2] John E. Gomez,[1] Benjamin Rodriguez,[1] John N Pham,[1] Clark Schiferl,[1] Christopher Rincon,[2] Cedric Bernier,[2] Caden Andersson,[1] Felicia Mendoza,[4] Jonathan Gasser,[1,5] Peter Wurz,[5] André Galli,[5] Eric Hertzberg,[1] and Nathan A. Schwadron[6]

AFFILIATIONS

[1]Space Science Division, Southwest Research Institute, San Antonio, Texas 78238, USA
[2]Mechanical Engineering Division, Southwest Research Institute, San Antonio, Texas 78238, USA
[3]Department of Physics and Astronomy, University of Texas at San Antonio, Texas 78249, USA
[4]Fuels and Lubricants Research Division, Southwest Research Institute, San Antonio, Texas 78238, USA
[5]Space Research and Planetary Sciences, Physics Institute, University of Bern, 3012 Bern, Switzerland
[6]College of Engineering and Physical Sciences, University of New Hampshire, Durham, New Hampshire 03824, USA

[a)]**Author to whom correspondence should be addressed:** justyna.sokol@swri.org

03 June 2024 15:15:42

ABSTRACT

We present diamond-like carbon (DLC) conversion surfaces to detect particles with energy below 2 keV. Conversion surfaces have been widely applied in measurements of low-energy particles by instruments onboard planetary and heliophysics missions. Their effectiveness is characterized by the efficiency in changing the charge state of the incident particles while maintaining a narrow angular distribution for the reflected particles. DLC as a conversion surface coating material has high conversion efficiency. We developed a conversion surface production process that provides ultra-smooth and ultra-thin DLC conversion surfaces. The process includes substrate preparation through precision cleaning, plasma immersion ion deposition of the DLC film, and diagnostics of the film parameters. The latter includes the measurement of the coating thickness, surface roughness, and the conversion efficiency for ion beams with energy below 2 keV. The process we developed provides the DLC conversion surface coating of repeatable parameters with a mean surface roughness of 3.4 ± 0.2 Å and a mean film thickness of 46.7 ± 0.8 nm uniform across the sample area. Ion beam measurements showed a negative ion yield of 1%–2% for hydrogen atoms and 8%–15% for oxygen atoms with an angular scatter distribution of 10°–20° at full width of half maximum. These results agree with those of other conversion surface coatings in the literature. The DLC conversion surfaces presented here are implemented in the conversion surface subsystem of the Interstellar Mapping and Acceleration Probe (IMAP)-Lo instrument of the IMAP mission scheduled for launch in 2025.

© 2024 Author(s). All article content, except where otherwise noted, is licensed under a Creative Commons Attribution (CC BY) license (https://creativecommons.org/licenses/by/4.0/). https://doi.org/10.1063/5.0203686

I. INTRODUCTION

Conversion surfaces, known also as ionization surfaces, have been extensively used in the space industry for decades (e.g., Wurz *et al.*, 1997; Scheer *et al.*, 2006; and Kazama *et al.*, 2007). They are a layer of a conversion material on top of an insulator or semiconductor substrate such as a silicon wafer (Fig. 1). The incident particles undergo a charge-exchange process within the solid material, which is used as one method for particle detection in low-energy plasma particle instruments (Wurz, 2000). Conversion surfaces enable the detection of neutral atoms and positive ions of energies below 2 keV through conversion to negative or positive ions and the release of secondary electrons (e.g., Wurz *et al.*, 2006; and Wahlström *et al.*, 2008; Fig. 1). They are also applied in ion beam neutralizers dedicated to creating a neutral atom beam used, e.g., during the calibration of the neutral atom instruments (Fuselier, 2009; and Gasser *et al.*, 2022). Moreover, the conversion

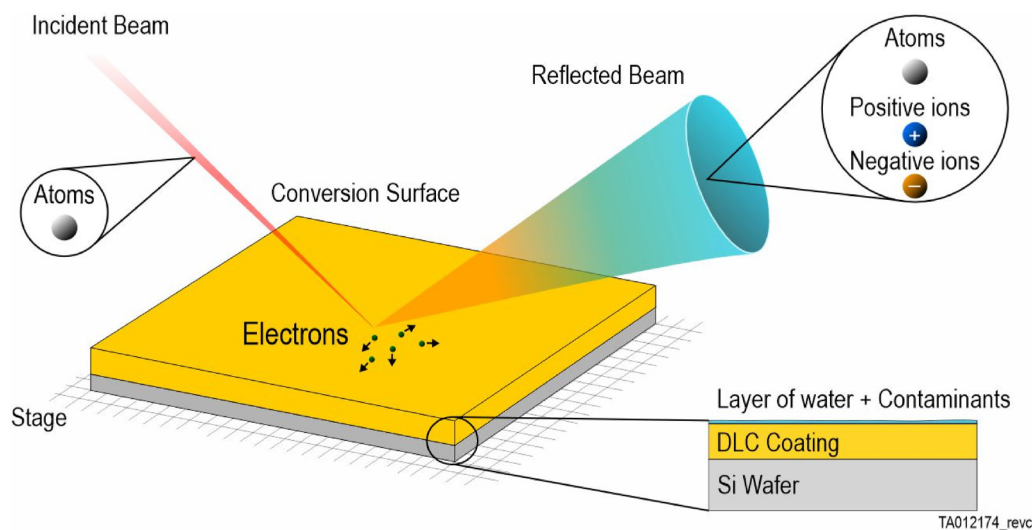

FIG. 1. Sketch of the scenario—not to scale: an incident beam of neutral atoms (or positively charged ions) hits the conversion surface (a layer of DLC film on top of a silicon wafer with a layer of contaminants on top) releasing secondary electrons and reflects as a beam consisting of sputtered and scattered products composed of atoms and negatively and positively charged ions.

surface detection technology has been demonstrated as the most effective method to study the neutral atoms of energies in the range of 10 eV–2 keV. Those atoms are very common in the plasma populations in planetary systems and interstellar space but are challenging to detect (Wieser *et al.*, 2002; and Neuland *et al.*, 2014).

Space plasma consists of particles of various energies and charge states. Planetary environments, interplanetary space, and interstellar medium are filled with atoms of energies ranging from a few eV up to MeV. Energetic neutral atoms (ENAs) are created in the charge-exchange process between ions and the ambient atoms and provide information about the plasma properties throughout the solar system, at the boundary regions of the heliosphere (a space filled by the solar wind in the interstellar medium), and in the interstellar medium surrounding the Sun (Hsieh and Möbius, 2022). Interstellar neutral (ISN) atoms are the neutral component of the local interstellar medium gas. They enter the heliosphere unaffected by the electromagnetic forces carrying information about the properties of the interstellar environment neighboring the Sun (e.g., chemical composition, plasma velocity distribution) and the Sun's motion in the galaxy. The neutral atoms have been measured in space since the 1960s (see, e.g., Neuland *et al.*, 2014 and references therein). Major planetary and heliophysics missions by space agencies across the world have used instruments to measure neutral atoms with conversion surfaces. Among them are Low-Energy Neutral-Atom Imager (LENA) (Moore, 2000) for IMAGE (Burch, 2000), GAS for Ulysses (Witte *et al.*, 1992), Interstellar Boundary Explorer (IBEX-Lo) (Fuselier, 2009) for IBEX (McComas *et al.*, 2009), Jovian Neutrals Analyzer (JNA) (Pontoni, 2022) at Jupiter ICy moons Explorer (JUICE) (Grasset, 2013), Neutral Particle Detector (NPD) for Mars and Venus Express (Barabash;, 2006,2007), Chandrayaan LENA (CENA) (Bhardwaj, 2005; and Kazama *et al.*, 2007) for Chandrayaan-1 (Bhandari, 2005), low-energy neutral atom (ENA) (Saito, 2010) for BepiColombo (Milillo, 2010), and Mars Ion and Neutral Particle Analyzer (MINPA) (Kong *et al.*, 2020) for Tianwen-1 (Ye *et al.*, 2017; and Wan *et al.*, 2020). Table I summarizes the listed missions and provides details on the mission's primary target and the type of conversion surfaces used.

The conversion surface material used in space instrumentation throughout the years varies depending on the instrument's design and measurement objectives of the mission. In general, the detection of an electrically neutral particle is possible, and most effective, when it is converted into an ion. Accelerating an ion to sufficiently high energy allows for mass and energy analysis far from the direct line of sight of any background. The conversion from neutral to the ion inside the ENA instrument is realized by two methods (Wurz, 2000): the atom passes through a thin conversion foil, e.g., a carbon foil (e.g., IBEX-Hi instrument, Funsten *et al.*, 2009), or the atom hits the conversion surface and is ionized by the surface ionization processes (e.g., LENA, CENA, IBEX-Lo). The foil conversion is applied to atoms with energies above about 1 keV, which have enough energy to pass through the foil, and the conversion through the surface ionization is applied to atoms with energies below 2 keV, which do not have enough energy to pass through the foil.

Conversion surfaces for space instruments should provide a high conversion efficiency, a product of ionization and reflection efficiency (e.g., Neuland *et al.*, 2014; and Gasser *et al.*, 2021). In the low-energy neutral atom instruments, they should have high efficiency in converting the incident particles into negative [e.g., diamond-like carbon (DLC) conversion surface at IBEX-Lo; Scheer *et al.*, 2006] or positive (e.g., CENA, JNA, and MINPA) ions with narrow angular and energy scattering distribution to prevent excessive flux reduction. Numerous studies of various types of conversion surfaces have shown that the smoother the surface of the

03 June 2024 15:15:42

© Author(s) 2024

TABLE I. Space missions with instruments using conversion surfaces.

Mission	Lifetime	Primary target	Instrument	Conversion surface material	Reference
IMAGE	2000–2005	Magnetosphere; ENAs	LENA	W	Moore, 2000
Ulysses	1990–2009	Heliosphere; ISNs	GAS	LiF	Witte *et al.*, 1992
IBEX	2008-present	Heliosphere; ENAs, ISNs	IBEX-Lo	DLC	Fuselier *et al.*, 2009
JUICE	2023-present	Jupiter system	JNA	Al_2O_3	Pontoni, 2022
Mars Express	2003-present	Mars	ASPERA-3/NPD	WO_2[a]	Barabash *et al.*, 2006; and Grigoriev, 2007
Venus Express	2005–2014	Venus	ASPERA-4/NPD	WO_2[a]	Barabash *et al.*, 2007; and Grigoriev, 2007
Tianwen-1	2020-present	Mars	MINPA	Al_2O_3	Kong *et al.*, 2020
Chandrayaan-1	2008–2009	Moon	CENA	MgO	Bhardwaj *et al.*, 2005; and Kazama *et al.*, 2007
BepiColombo	2018-present	Mercury	ENA	Al_2O_3	Saito *et al.*, 2010; and Kazama *et al.*, 2007
IMAP	2025 (planned)	Heliosphere; ENAs, ISNs	IMAP-Lo	DLC	McComas *et al.*, 2018

[a]The start surface is a multi-layer coating composed of a thin layer of Cr_2O_3, covered by a thicker layer of MgF and topped with a thin layer of WO_2, and the stop surface is part of a graphite sphere (roughness around 100 nm) covered by a MgO layer of ∼500 nm thickness. ASPERA—Analyzer of Space Plasma and Energetic Atoms, CENA—Chandrayaan LENA (low-energy neutral atom), ENA—Energetic Neutrals Analyser, IBEX—Interstellar Boundary Explorer, IMAP—Interstellar Mapping and Acceleration Probe, IMAGE—Imager for Magnetosphere-to-Aurora Global Exploration, JUICE—Jupiter ICy moons Explorer, JNA—Jovian Neutrals Analyzer, LENA—Low-Energy Neutral-Atom Imager, MINPA—Mars Ion and Neutral Particle Analyzer, NDP—Neutral Particle Detector.

conversion film, the more effective the conversion and transmission of the ions into the subsequent subsystems of the instrument. Thus, the conversion surfaces should be extremely smooth (with surface roughness less than 1 nm) to prevent the secondary scattering of the surface and keep the properties of the incident particles unchanged. The material of the conversion surfaces should have good particle reflection properties, be preferably made of high-Z compounds, and demonstrate a good suppression of the UV light against forward scattering into the particle instrument system (e.g., Barabash, 2006; Wurz *et al.*, 2006; and 2008). In addition, the performance of the conversion surface should remain stable over the life of the mission, it should not degrade in time and changing operation environments.

Southwest Research Institute (SwRI; Southwest Research Institute, 6220 Culebra Road, San Antonio, TX 78238-5166, USA; swri.org) has developed a process for DLC coating on silicon substrates that provides ultra-thin (film thickness below 50 nm) and ultra-smooth (surface roughness Rq≤5 Å) conversion surfaces. Those conversion surfaces have been used for the conversion surface subsystem of the IMAP-Lo instrument onboard the Interstellar Mapping and Acceleration Probe (IMAP; McComas *et al.*, 2018) mission, which is scheduled for launch to an orbit at L1 in 2025. The IMAP-Lo instrument will measure ISNs of H, He, Ne, O, and D, as well as heliospheric ENAs of H for energies from 0.01 to 1 keV (McComas *et al.*, 2018; Sokół *et al.*, 2019; and Schwadron *et al.*, 2022). Its concept is based on the IBEX-Lo instrument (Fuselier, 2009) of the IBEX mission (McComas *et al.*, 2009). IBEX-Lo detects neutral particles through DLC conversion surfaces manufactured by Lockheed Martin Advanced Technology Center, Sandia National Laboratories, and the University of Arizona (see Fuselier, 2009). These DLC conversion surfaces have demonstrated high surface smoothness, stability over time, and resistance to damage, similar to a pure diamond. IBEX-Lo conversion surfaces have a 100 nm thick DLC coating with a surface roughness near Rq = 1 Å. They have shown conversion efficiency higher than other materials (Scheer *et al.*, 2006; Wieser *et al.*, 2007; Wahlström *et al.*, 2008; and Wurz *et al.*, 2008) and highly stable performance since the beginning of the IBEX-Lo operation in late 2008 and continuing into 2024.

03 June 2024 15:15:42

Continuing the successful implementation of DLC conversion surfaces on IBEX-Lo, IMAP-Lo also will use DLC conversion surfaces. The IMAP-Lo's conversion surface subsystem consists of 28 DLC-coated facets cut out from highly polished silicon wafers. However, since the technology applied to produce the IBEX-Lo conversion surfaces was no longer available, the production process of the ultra-thin and ultra-smooth DLC coating had to be developed again. In this paper, we report on the production process of the IMAP-Lo DLC conversion surfaces and their characteristics. In Sec. II, we describe the methods and measurement techniques we used including substrate selection (Sec. II A), substrate preparation for coating (Sec. II B), requirements for storage and transport (Sec. II C), atomic force microscopy (AFM) for surface roughness (Sec. II D), DLC coating (Sec. II E), variable angle spectroscopic ellipsometry (VASE; Sec. II G), and beam measurements (Sec. II G). In Sec. III, we present and discuss the results of the production process for the ultra-thin and ultra-smooth DLC conversion surfaces, and in Sec. IV, we summarize the study.

II. METHODS AND TECHNIQUES

Manufacturing of the DLC conversion surfaces is a multi-step process consisting of substrate dicing, cleaning in preparation for

© Author(s) 2024

coating, conversion film deposition, and measurements of the coating quality for film smoothness, thickness, and conversion efficiency properties, as illustrated in Fig. 2. The DLC conversion surfaces made by SwRI are the DLC film deposited on a highly polished silicon wafer, which serves as a substrate (see more details in Secs. II A and II D). The wafers are diced to a shape required by the project. The dicing process requires protecting the surface from scratches and damage, which can alter the ultra-smooth surface of the wafer. Before deposition of the conversion film, the substrates are precision cleaned to remove particle contamination and the oxide layer from the front surface (more in Sec. II B). Once cleaned, the polished side of the wafers was coated with a thin DLC layer through Plasma Immersion Ion Deposition (PIID; Sec. II E). Next, the quality of the coating is verified with the measurements of the film thickness (Sec. II F), surface roughness (Sec. II D), and charge-conversion efficiency (Sec. II G).

A. Substrates

The silicon wafers used as the substrates for the IMAP-Lo conversion surfaces were provided by Virginia Semiconductor Inc. They are 3 in. (7.62 cm) diameter wafers, grown with the Czochralski process, Boron doped, with primary flatness, single-side polished with the backside etched, and the polished surface roughness rms ≤ 5 Å as ordered. AFM measurements of the surface roughness of the Si wafers confirmed their surface roughness Rq ≤ 5 Å. However, the measurements showed that the surface roughness varies from the center of the wafer toward the edge by about 2 Å. The concentric variation in the surface roughness is presumed to be related to the polishing method of the wafers to the requested smoothness.

Next, each wafer was diced into a trapezoid-shaped piece, a facet (see Fig. 3), from the central part of the wafer to meet the IMAP-Lo instrument design requirements. The dicing process requires a means to protect the polished surface against damage (e.g., scratches) and contamination as well as keeping edge chips below 25 μm in size. A dicing process meeting the requirements was provided by Micro Precision Engineering (MPE, Greenville, TX, USA). In addition to the facets, 2 cm square pieces were diced from the wafer remainder. These square pieces were processed in parallel with the facets to become the test samples for the conversion efficiency measurements (more in Sec. II G). After dicing, the substrates were inspected at SwRI for surface roughness (with AFM) and edge finishing (with optical and digital microscopes).

B. Substrate preparation

In preparation for the coating, the substrates were precision cleaned to remove the remnants of the surface protection material from the dicing process and provide a surface free from particulates (within requirements), which could adversely affect the adhesion and the smoothness of the coating. Precision cleaning was performed in a cleanroom (ISO-6) using a two-step process including wet and dry cleaning techniques. The wet cleaning included

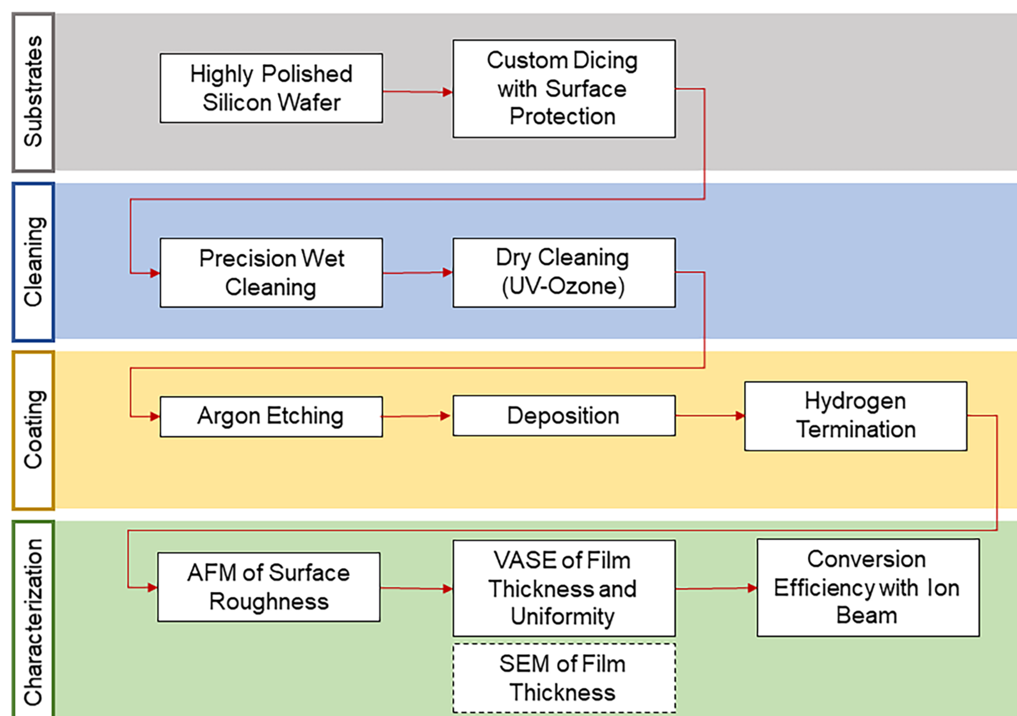

FIG. 2. Production flow chart for ultra-smooth and ultra-thin DLC conversion surfaces for space application.

03 June 2024 15:15:42

© Author(s) 2024

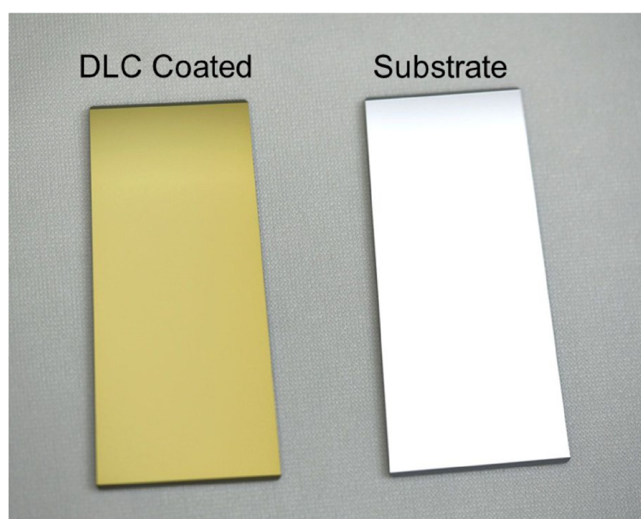

FIG. 3. Conversion surface facet before (right, saturated due to very high reflectiveness) and after (left) DLC coating. The DLC-coated surface has a golden color. Photograph taken with ambient cleanroom fluorescent light.

blowing off particulates from the surface using nitrogen, rinsing with de-ionized (DI) water with a resistivity larger than 15 MΩ, and rinsing with high-purity isopropyl alcohol (IPA). Both DI water and IPA are well known for their cleaning properties and are commonly used in numerous non-invasive cleaning processes. The DI water and IPA rinses were repeated several times, and the process was completed with nitrogen to blow dry the surface.

After the first stage of wet cleaning, the surface was inspected under an optical microscope (e.g., Luxo Microscope by Unitron) for signs of remaining contamination and marks from cleaning solution drying. If the surface did not meet cleanliness requirements, either the DI water and IPA rinses were repeated or an IPA or acetone wipe was performed depending on the amount and type of contamination remaining on the surface. For the wiping stage, only dry cleanroom sealed-border wipers made from 100% polyester are used (e.g., TX1010 Vectra Alpha 10). These wipers do not adversely affect the surface as they have been tested for snagging, surface abrading, and release of particles and fibers. For the IPA and acetone wipe, the wiper was dampened in the solution and the surface was manually cleaned with the contact area of the wiper changed after every wipe. Since both IPA and acetone are solvents and can dissolve the gloves and wipers, the process was monitored to ensure no contamination from these materials.

Dry cleaning was performed once wet cleaning was acceptable. We used UV-ozone cleaning to remove any organics left on the surface of the substrates. UV-ozone cleaning is a cleaning process commonly used in surface processing. It has been proven as a highly effective non-acidic, dry, and non-destructive atomic cleaning and organic removal process and, thus, improves surface adhesiveness. For this cleaning, ultraviolet light with 185 and 254 nm wavelengths are used. The 185 nm light is used to produce ozone from the oxygen present in the air. The 254 nm light dissociates ozone creating singlet atomic oxygen, which has strong oxidation power and reacts with molecules and organics residues on the substrate's surface removing them in the volatile form. This provides contamination removal within minutes without damage to the surface. The effectiveness of the cleaning can be improved by increasing the stage temperature, which improves the density of the reactive species and accelerates the cleaning rate. During the UV-ozone cleaning of the substrates, we placed them at a distance of about 30 mm from the double tube low-pressure mercury lamps on an aluminum tray preheated to about 30 °C and cleaned the substrates for 16 min with the temperature increasing during the process. The temperature of the substrates' holder at the end of the cleaning process was typically in the range of 40–50 °C. The UV-ozone cleaner unit we used did not allow for temperature control; however, we have verified that the mild cleaning conditions applied were enough to prepare the substrates for the film deposition. We observed surface roughness by about $\Delta Rq = 0.1$ nm less after applying the UV-ozone cleaning to the substrates.

The UV-ozone cleaning completed the preparation of the substrates for coating. After cleaning, the substrates were transported to the deposition chamber in which the coating process was performed (Sec. II E). The cleanliness of the substrates' surface as well as of the coated substrates (conversion surfaces) was monitored at various stages of the production process using standard flashlight inspection. At random, and when necessary, inspection with an optical microscope was performed.

The DLC-coated substrates sometimes required cleaning at various stages of measurements of the film properties. For that, wet cleaning with DI water and IPA rinse (and a mild wipe when necessary) was performed. The cleaning was applied to remove the large-scale particles originating mostly from the air and handling outside the cleanroom and, thus, were on top of the coated surface. The middle panel of Fig. 4 presents an AFM analysis for a coated surface with on-top contamination. The surface roughness for the entire scanning area (see more in Sec. II D) in this instance was $Rq = 2.68$ nm due to the large-scale particles biasing the results. After wet cleaning, the measured surface roughness was $Rq = 0.35$ nm.

The coated surfaces were protected from surface and film damage at all times. In addition, as demonstrated by Riedo *et al.* (2010), long-duration UV irradiation of the DLC conversion surfaces causes degradation of the performance of the conversion efficiency of the conversion surfaces due to the build-up of a permanent hydrocarbonaceous layer on the surface. Thus, a limitation of the exposure of the DLC coating to the light was highly recommended after the deposition process with special precautions for exposure to the UV light of wavelengths below 200 nm. Thus, protective, light-blocking containers were used for the transport and storage of the IMAP-Lo conversion surfaces (Sec. II C).

C. Storage and transport

The substrates and the coated parts were frequently transported between various facilities engaged in the production process. Thus, containers for the storage and transport of the substrates and the coated conversion surfaces should fulfill several requirements. First, they should protect the highly polished surface of the substrates from any type of damage (including scratches)

03 June 2024 15:15:42

© Author(s) 2024

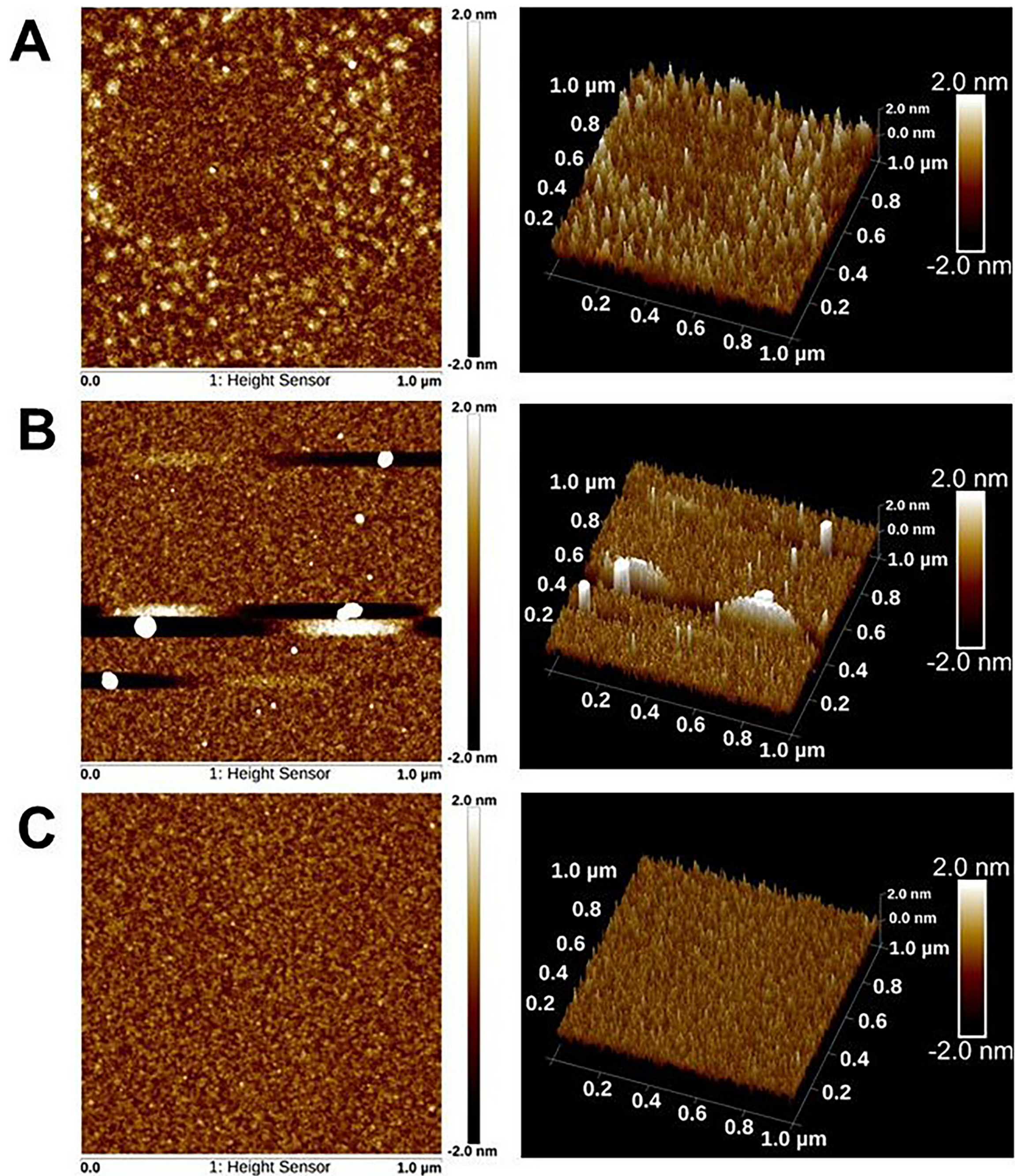

FIG. 4. AFM image (2D left column, 3D right column) of the DLC film with surface contamination [top (A) and center (B)] and without surface contamination [bottom (C)] for the probing area of 1 μm^2. The surface roughness (Rq) of the entire scanning is 0.47 (A), 2.68 (B), 0.33 nm (C).

and protect the edges and corners of the parts from damage. Second, they should reduce excess motion of the samples inside the container during the transportation that could result in damage to the edges of the facets or square test sample and scratching of the highly polished surface. Third, they should protect the conversion surface from exposure to UV light (Riedo *et al.*, 2010). Finally, the containers should be reusable and easy to clean and allow for effortless loading and unloading of the samples inside them.

03 June 2024 15:15:42

© Author(s) 2024

Several types of containers were considered and tested during the development process. Gel-Pak containers commonly used in the silicon industry were ruled out early in the development phase because they do not allow for multiple usage since the dust and contamination particles could easily get trapped on the gel and, thus, increase the risk of transfer of contaminants on the substrates. Another type of container considered for long-distance transport of the parts (from the dicing facility to SwRI), especially the customized facets, was the aluminum cassette. However, they required retainers to securely fix the samples to the cassette, which required force and, thus, increased the risk of damage to the edge of the fragile parts. Thus, containers made of softer materials were considered. One of them was the polypropylene coin containers commonly used for wafer shipment. They performed surprisingly well for long-distance transport of the samples since placing the substrates with the polished surface downward protected them from unwanted scratching, thanks to the beveled edges of the facets. However, they were ruled out as storage and transport containers for the coated conversion surfaces because of several reasons. Mainly, loading and unloading facets to and from the coin containers was troublesome and frequently resulted in contact with the surface.

The solution settled on was trays designed to hold multiple facets that allowed for effortless loading and unloading of the parts and secure transport between facilities throughout the SwRI campus. First, the trays were 3D-printed in Ultem, which is a softer material and, thus, reduces the risk of damage to the edges and corners of the facets. However, the 3D-printed Ultem containers unexpectedly contaminated the samples. The detergent solution used to clean these trays was trapped within Ultem. The detergent remained after a long vacuum bake and eventually dissipated out and settled onto the facets. As a result, they were not a viable solution for long-term or short-term conversion surface storage. Subsequently, trays made of aluminum 6061-T651 and flashed with electroless nickel were used for short-distance transportation (within the SwRI campus) and long-term storage. As this container was used only for controlled short-distance transportation, the aforementioned facet retainers were not implemented, which reduced the risk of damage. To further reduce contamination risk, the containers were cleaned via sonication with DI water and detergent, DI water rinsed, and vacuum baked. Cleanliness was confirmed with a quadrupole mass spectrometer scan.

The container along with substrates and conversion surfaces were stored in an N_2 purge cabinet whenever possible to satisfy a controlled dry environment. Additionally, for any intermediate relocation of the parts from their containers, a vacuum wand was used along the unpolished backside of the facet to prevent unnecessary contact with gloved hands.

D. AFM

AFM, first developed by Binnig *et al.* (1986), is a high-resolution topographical imaging technique used for surface analysis at the nanometer spatial scale. AFM systems scan sample surfaces with a sharp probe tip mounted on a flexible cantilever, detecting surface features through force interactions between the tip and the sample. As the tip responds to atomic forces at each pixel, atomic force interactions are measured by a laser beam deflection to produce a topographical map (Garcia and Perez, 2002). As the probe moves along the scanning surface, the deflection of the probe cantilever is used to measure interaction forces with the sample at each pixel and generate high-resolution topographical maps, which are used to acquire the surface's root mean squared roughness (rms or Rq, the root mean squared average of the profile height over the evaluation length) and average roughness (Ra, an arithmetic average of the absolute values of the profile heights over the evaluation length). Ra measures the absolute deviations from the mean height, meaning that it does not distinguish between peaks and valleys. Rq measures the average deviation of height values from the mean surface height and is more sensitive than Ra to positive and negative outlier height deviations (Kumar *et al.*, 2012), such as those presented by contaminant particles. To better quantify particle contamination on surface coatings, Rq was selected as the primary roughness measure.

Thus, AFM allows for the measurement of high-resolution, three-dimensional topographical maps of samples at the nanoscale, which are used to precisely measure surface roughness. For this study, AFM measurements were performed with a Bruker Nanoscope V Dimension ICON unit equipped with a Bruker SCANASYST-AIR scanning probe (parameters of the probe tip radius: 2 nm, length: 115 μm, width: 25 μm, frequency: 70 KHz, spring constant: 0.4 N/m). The probe selection, scanning mode (PeakForce Tapping), and mode settings were optimized for surface roughness below 5 Å based on guidance from Bruker. The PeakForce Tapping mode was selected over traditional tapping or contact scanning modes as it enables better control over probe-to-sample interaction, allowing for high-resolution scans while simultaneously minimizing imaging forces to protect the sample surface against contact. AFM tapping modes utilize intermittent contact with the surface to minimize lateral forces compared to the contact mode but can still cause damage to fragile samples during scans (Simpson *et al.*, 1999). The PeakForce Tapping mode, developed by Bruker in 2009, taps the sample with the probe tip at a set frequency while maintaining a specified maximum force, enabling precise control over probe-to-sample interaction forces and, thus, protecting delicate coatings while providing the highest resolution scans (Hardij *et al.*, 2013).

The AFM's sensitivity to changes in the surface height allows for detecting and measuring particle contamination on smooth DLC surfaces, making it particularly useful for developing an effective cleaning process (Sec. II B). Moreover, after consultation with Bruker, we replaced the scanning probe after every 20 scans to avoid biasing the surface roughness measurements due to tip wear. The 20 scan limit of the scanning probe satisfies stable surface roughness measurements within 0.02 nm standard deviation.

During the production of conversion surfaces, witness facets and test samples were used throughout the DLC deposition process to measure the coating surface roughness. We scanned the samples at five (square test sample) and nine (facet) evenly distributed locations across the sample area to ensure the consistent verification of the surface properties within a reasonable data acquisition time. Each location had a scanning area of 1 μm^2, and the measured surface roughness was reported as Rq in Å (see Fig. 4). The acceptance range of the surface roughness for a given sample was Rq less

03 June 2024 15:15:42

© Author(s) 2024

than or equal to 10 Å for the mean value from all the scanning locations. Conversion surfaces with a surface roughness of 10 Å or larger showed wide angular scatter distribution of the reflected ion beam, which significantly reduces the conversion efficiency of such a coating (see more in Sec. III).

E. Coating

The DLC conversion film on IMAP-Lo conversion surfaces was deposited using the PIID method, which is an advanced version of the Plasma Enhanced Chemical Vapor Deposition (PECVD) technique. The PECVD has been widely used in the industry since its first application in the 1960s (Sterling and Swann, 1965). In this technique, the source material is supplied to the sample surface in the form of gaseous compounds. Precursor gas molecules decompose at the surface leaving the desired species (e.g., Oura *et al.*, 2013). The DLC film deposition process applied to IMAP-Lo conversion surfaces has been optimized to provide the DLC film of surface roughness below 5 Å with simultaneous film thickness around 45 nm.

The PIID process was carried out in a cylindrical vacuum chamber with a diameter of 1.22 meters and a length of 2.4 meters. A portable soft wall cleanroom (ISO-7) was assembled at the entrance to the chamber. Thanks to it, the substrates were prepared for installation inside the chamber in an environment with controlled cleanliness. The particle monitor inside the cleanroom indicated ISO-5 during the process of sample installation inside and taking out of the chamber. In addition, the technicians responsible for sample handling before and after the coating process follow the cleanroom and contamination control procedures. Contamination control was an essential requirement for the entire deposition process. After the substrates were precision cleaned (Sec. II B), their surfaces must be kept clean; however, the cleaning and coating were performed in separate facilities requiring transport. The transport and installation of the substrates inside the chamber were performed by hand. To reduce contamination exposure while unpacking the samples from their storage carriers in the coating facility, the cleanroom was used. Any contamination of the pre-cleaned surface of the substrates before the deposition would result in a reduction in the film adhesiveness or an increase in the surface roughness.

The pre-cleaned IMAP-Lo conversion surface facet and square test sample substrates were placed on an aluminum foil-covered flat sample alignment plate in the center of the chamber (Fig. 5). Up to 16 facets could be coated in one deposition process. The substrates were placed on an area of the plate that provided a uniform film thickness of approximately 45 nm and a surface roughness of less than 10 Å for every sample with a variation of less than 5 nm and 2 Å, respectively. The square test samples were placed in spaces between the facets within the uniform coating area on the plate to better serve as the witness sample.

The application of the DLC film comprised three processes: argon plasma etching, DLC deposition, and hydrogen termination. The three processes were performed one after the other during the coating processes. After pumping down the vacuum chamber to below 1.33×10^{-3} Pa, Ar gas was fed into the chamber to reach a pressure of approximately 2 Pa. A train of negative pulsed voltage

FIG. 5. Holding plate with conversion surface substrates during the deposition process.

03 June 2024 15:15:42

was applied to the samples at 4 kV with a pulse frequency of 2000 Hz and a pulse width of 20 μs to generate an argon plasma to clean the sample surface for 15 min. The argon plasma cleaning process is commonly used to remove native oxides and absorbed contaminates on the surface without modifying the surface being treated. The duration of the argon plasma cleaning has been determined in the development process and was accordingly adjusted to clean the substrates without altering the surface roughness of the substrates, which can happen if the argon plasma cleaning is too intensive. Next, acetylene (C_2H_2) was introduced into the vacuum chamber to deposit the DLC film at the same working pressure inside the chamber of 2 Pa. The pulsed voltage remained at 4 kV with the same pulsing parameters during the DLC film deposition. The DLC film deposition time was determined to be 15 min to provide the DLC film thickness of about 45 nm. After applying the DLC film, hydrogen termination was performed for 15 min using the same pulsing voltage with a hydrogen (H_2) plasma at 2 Pa. Hydrogen termination was applied to remove dangling bonds of the diamond lattice and, thus, reduce the reactiveness of the surface that could adversely affect the surface roughness. The hydrogen termination completed the coating process. After DLC film

© Author(s) 2024

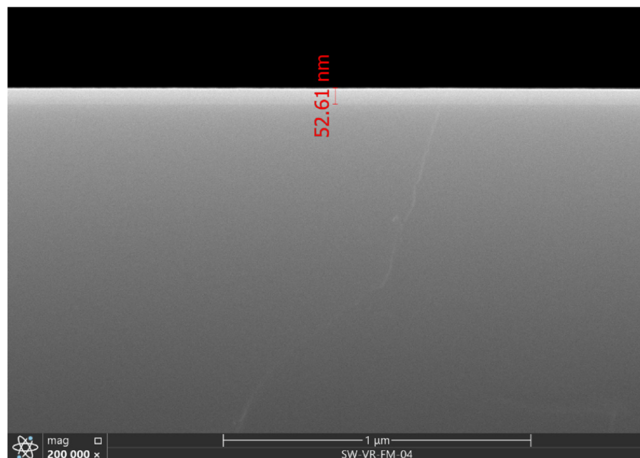

FIG. 6. Example of SEM measurement of the thickness of the DLC film on top of the silicon wafer performed in the development process. The VASE measurements indicated the film thickness for that the sample ranging from 51.00 to 51.36 nm depending on the DLC model used in the measurement interpretation. The difference of a few nm is within the measurement accuracy of both techniques for such thin films.

application, the chamber was vented to atmospheric pressure using a cleanroom grade of nitrogen (N_2). Due to the large volume of the UHV chamber used in the coating process, both pumping down and venting were performed at a low rate to reduce any unnecessary motion of particulates inside the chamber that could settle on the substrates. If particulates settle down on the substrates before the deposition process begins, they could be coated and, in consequence, reduce the film adhesiveness or increase the surface roughness. Samples with visible signs of coating contamination by particulates under the film were not qualified as conversion surfaces.

The DLC-coated conversion surface facets and square test samples were transferred to storage trays immediately after venting the chamber. The witness facets and square test samples were separated from the remaining facets and forwarded for film diagnostics, including the measurement of the film thickness (Sec. II F) and surface roughness (Sec. II D).

F. VASE

The DLC film thickness of the conversion surfaces was measured using a J.A. Woollam M-2000 variable angle spectroscopic ellipsometer (VASE). It is a non-destructive technique using a beam of polarized light with a wavelength typically ranging from 400 to 1700 nm. As the beam strikes the surface, the beam splits into a reflective portion and a refractive portion. The refractive portion of the beam depolarizes as it passes through the film and reflects off the substrate, and the degree of depolarization is measured by the instrument. The degree of light depolarization is expressed as functions of psi (amplitude ratio) and delta (phase difference) across the wavelength range. The experimental data are plotted, and a model is used to recreate the plot to calculate the film thickness. In general, ellipsometry is used to determine the film thickness, and optical constants, and characterize composition, crystallinity, and other material properties associated with a change in the polarization of the reflected and transmitted light (Woollam *et al.*, 1999; and Johs *et al.*, 1999). Currently, ellipsometry allows for the measurement of nanometer-scale layers and, thus, the range of its applications is very broad.

The incidence angle is a critical factor in the VASE analysis to allow for the polarized light to refract into the film. For the DLC film, we used incident angles between 50° and 70° capturing data in increments of 5°. The experimental data have been collected from numerous points across the sample area (35 for the facet and 25 for the square test sample) to probe the film thickness at different locations at the sample surface as well as to measure the film thickness variation across the sample area. After the experimental data had been collected, data analysis through the Woollam CompleteEASE software was used to determine the film thickness (CompleteEASE™ Data Analysis Manual by J.A. Woollam Co. Inc.). For that, a model is used to calculate the predicted response from Fresnel's equations, which describe each material with thickness and optical constants (refractive index and extinction coefficient). Known parameters for the substrate (e.g., 1 mm thick silicon wafer without oxide layer) and the coating (e.g., a single layer of DLC) are introduced to the system as initial parameters for preliminary calculations. The calculated values are compared through regression analysis to experimental data available in the Woollam CompleteEase software library. For the DLC, three models were evaluated: DLC-Hi, DLC-Lo, and DLC-CodyLor. Of the three available DLC models assuming DLC for different densities and properties, the DLC-Hi model best characterized the type of DLC formed during deposition. The DLC film has not been measured for the coating density and the sp2/sp3 bond ratio, and, thus, the best model selection was determined based on the independent film thickness measurements with scanning electron microscopy (SEM) for a few selected samples during the development phase of the project. The SEM method probes the film thickness based on the imaging of the cross section of the sample (Fig. 7), which requires breaking of the sample. This made it an unacceptable diagnostic technique for film thickness measurements of the witness facets and square test samples since subsequent use of these pieces was needed. Thus, the VASE technique was used as the primary method to measure the thickness of the coating because it is noninvasive and, thus, does not alter the surface of the sample. Figure 6 presents an example of the SEM measurement result for a film of about 52.61 nm thickness. The VASE measurement for this sample indicated a film thickness in the range of 51.00–51.36 nm. The difference of a few nm is within the measurement accuracy of both techniques for such thin films.

Figure 7 illustrates the outcome of the VASE measurements for two samples, a 3 in. in diameter silicon wafer with a nonuniform film thickness variation of 4 nm and a conversion surface facet with a uniform film variation of 1 nm. The nonuniform results for the film thickness can be the result of several factors, including non-uniform coating or contamination present on top or under the film. The contamination, especially when it covers a broad area, can manifest as an extra layer of material that disturbs the light path and is not included in the model used in the data interpretation. The acceptance range for the film thickness was 35–55 nm for the mean calculated from the measurement points.

03 June 2024 15:15:42

© Author(s) 2024

G. Conversion efficiency measurements

The quality of the conversion surfaces for space applications is determined by their ion yield, which is efficient in converting neutral atoms into positive and negative ions (e.g., Gasser *et al.*, 2021). Depending on the details of the instrument detection technique, either negative (e.g., IBEX-Lo, IMAP-Lo) or positive (e.g., JNA/JUICE, MINPA/Tianwen-1) ions are utilized. The parameter complementary to the ion yield is the angular scatter distribution of the particles reflected off the conversion surface (see Fig. 1). The narrower the cone of the reflected beam, the better the performance of the conversion surface for particle detection is. The narrow distribution of the reflected products means that fewer particles are lost in the ion-optical system used for mass and energy analysis and, thus, increases the throughput of particles entering the instrument's subsystems following the conversion surface.

The Imager for Low Energetic Neutral Atoms (ILENA) facility of the University of Bern in Bern, Switzerland, is a test facility to study surface-interaction processes for particle detection in space through conversion surfaces (Wahlström *et al.*, 2013; Gasser *et al.*, 2021; and Gasser, 2023). The ILENA setup has an electron impact ion source to provide an ion beam, a sector magnet for ion species selection, and a 2D multichannel plate (MCP) imaging detector. During the tests, positive ions are produced and extracted by a post-acceleration voltage to a few 100 eV/q from the ion source. The ion beam is focused and guided into the sector magnet, where the ion species is selected by mass-per-charge according to the magnetic field and chosen ion energy. The ion beam passes through a 1 mm diameter pinhole before it strikes the conversion surface sample under a grazing incidence angle, by default at 8° to the sample surface (at 82° to surface normal). A weak magnetic field parallel to the conversion surface sample is used to deflect secondary electrons released from it during interaction with the ion beam. After the charge-exchange interaction of the ion beam with the surface, the particles such as positive and negative ions and neutral particles are scattered toward the MCP detector. Appropriate adjustment of the positive electrostatic potential on the retarding potential analyzer (RPA) installed in front of the imaging detector prevents positive ions from reaching the detection subsystem and suppresses low-energy electrons by a slight negative potential grid. In consequence, only neutral atoms and negative ions are registered by the imaging detector.

The negative ion yield η is computed from the numbers of neutral atoms (N_0) and negative ions (N_-) scattered off the conversion surface sample [$\eta = N_-/(N_0 + N_-)$], where the number of registered atoms and ions is a function of detection efficiency and the number of registered counts (see more details in Gasser *et al.*, 2021; and Gasser, 2023). The angular distribution of the reflected beam is measured through the 2D MCP detector. The full width at half maximum (FWHM) in azimuth (tangentially to the surface) and polar (normal to the surface) direction is registered at various incident energies by reading out the extent of the 50% contour line in the angular distributions.

For the IMAP-Lo DLC conversion surface, the negative ion yield η has been determined for hydrogen and oxygen at a few energies in a range from 200 to 1000 eV per atom. To account for and subtract the negative ion contributions from particle sputtering off the conversion surface, the same measurement has also been conducted using the noble gases helium and neon. The noble gases do not form stable negative ions, and, thus, neutral noble gas atoms cannot be directly detected using the charge-conversion methods. They can only be detected indirectly by their sputtering of surface atoms (the so-called sputter contribution, see Sec. III). For hydrogen at energies below 600 eV and oxygen below 400 eV, molecular ions (H_2^+, O_2^+) at twice the nominal energy have been used as the source beam (see Gasser *et al.*, 2021).

III. RESULTS AND DISCUSSION

After the completion of the coating process (Sec. II E), the IMAP-Lo DLC conversion surfaces were tested for film thickness and uniformity (Sec. II F), surface roughness (Sec. II D), and conversion efficiency (Sec. II G). Each of these quality measurements was performed in different facilities and at different times; the film thickness and surface roughness were measured typically within 24 h after the film deposition, all at SwRI but in different buildings. The conversion efficiency measurements were performed a few months after the completion of the coating at the University of Bern. In addition, every one of those measurements required significant time to acquire the data and analyze the results. Thus, the measurements were performed on selected reference conversion surface samples, the witness facets and square test samples, to track the properties of the conversion surfaces throughout the entire process. Using the witness facets for the quality measurements saved time and money and, more importantly, prevented the final conversion surfaces intended for installation on the flight IMAP-Lo unit from unwanted contamination, e.g., due to operation in a non-cleanroom environment and transport between facilities.

03 June 2024 15:15:42

Ten sets of flight model (FM) conversion surfaces have been coated with DLC film. This coating process resulted in 70 potential flight facets, 10 witness facets to track the DLC film surface roughness and film thickness, and 10 square test samples to measure the DLC film surface roughness, film thickness, and conversion efficiency. Conversion efficiency measurements were performed only on the squared test samples since the ILENA setup has limitations on the sample size that could be installed inside the test chamber.

The results of the first coating attempts showed that the DLC film thickness of 100 nm as it was for the IBEX-Lo conversion surfaces has surface roughness larger than 10 Å. Such surface roughness adversely affected the angular width of the reflected beam by making it wider reducing the conversion efficiency of the conversion surfaces and, thus, the detection efficiency of the instrument (e.g., geometric factor). In general, a narrower angular distribution of the reflected beam in the polar and azimuth directions results in a more collimated beam of converted ions. This allows a more effective collection of the beam by the steering magnets toward the post-acceleration subsystem (Fuselier *et al.*, 2009). The reduction in the DLC film thickness resulted in a reduction in the surface roughness and, in consequence, the narrowing of the angular distribution of the reflected beam. Initial results indicated that the DLC film of 40 nm provides surface roughness that reproduces the conversion efficiency of the IBEX-Lo conversion surfaces.

© Author(s) 2024

Further improvements in the production process, including precision cleaning of the substrates in preparation for the coating, and contamination control throughout the entire coating and diagnostic process, resulted in DLC conversion surfaces showing conversion efficiency comparable with IBEX-Lo conversion surfaces. We developed a process for conversion surface production that provides conversion surfaces with repeatable parameters of a mean surface roughness of Rq = 3.4 ± 0.2 Å uniform among the coated area and a mean DLC film thickness of 46.7 ± 0.8 nm uniform across the coated substrate.

Selected conversion surface square test samples were characterized for conversion efficiency in the ILENA facility (Sec. II G). Two engineering model (EM) and three FM conversion surface samples were measured for incident beams of hydrogen, helium, neon, and oxygen. The negative ion yield and angular scatter distribution in polar and azimuth directions were determined as presented in Fig. 8. All samples show consistent results for the negative ion yield and the angular scatter distribution within the statistical variation and measurement accuracy of the test facility.

In Fig. 8, the negative ion yield, η, for impacting hydrogen and oxygen beams represents the values that are corrected for the sputter contribution. For He and Ne, the shown η represents the sputter yield of negative ions instead of direct charge-conversion efficiency. Measurements were done at energies per atom: 195, 250, 390, 500, 780, and 1000 eV. The measurement series for H and He labeled FM-061r are repeated measurements for sample FM-061 to validate the uncertainty of the experiment conditions in the first measurement run. Missing data points in the azimuthal FWHM plots indicate that the distribution half maximum was beyond the measurement range of the imaging detector, which is 21° × 21°. The measured values for η are in agreement between the tested samples within the experiment uncertainties. For all tested samples, η values are within the range $\eta_H = 2\% \pm 0.5\%$, $\eta_O = 9\% \pm 0.5\%$ at 200 eV and $\eta_O = 13.5\% \pm 1.5\%$ at 1 keV. The sputter contributions are in a range from 1.5% to 3% for He, and from 3% to 5% for Ne (Fig. 8).

The angular distribution widths show discrepancy for a few data points, e.g., sample EM-039 shows considerably narrower He and Ne scatter than the rest, and the oxygen azimuth FWHM for sample EM-036 is about 2° larger. The three tested FM conversion surface samples show scatter distribution results mutually in agreement. A few single misaligned data points (He at 780 eV) should be considered outliers. Apart from these, the results presented in Fig. 8 show consistent angular scatter between the tested samples. Given the high requirements on sample positioning accuracy in the ILENA as well as on the stability of the experiment conditions, the deviations in angular scatter distribution widths observed are rather an artifact of the limited precision of the experiment setup than a sign of considerable structure variations among the conversion surface test samples.

The measurement uncertainties of the scatter width equal to ±0.5° are empirically determined estimates based on the accuracy of reading the contour plot of the accumulated angular scatter distribution. The uncertainty of the negative ion yield was determined empirically by repetition several times at the same measurement point under constant conditions and concluded to be ±0.5%.

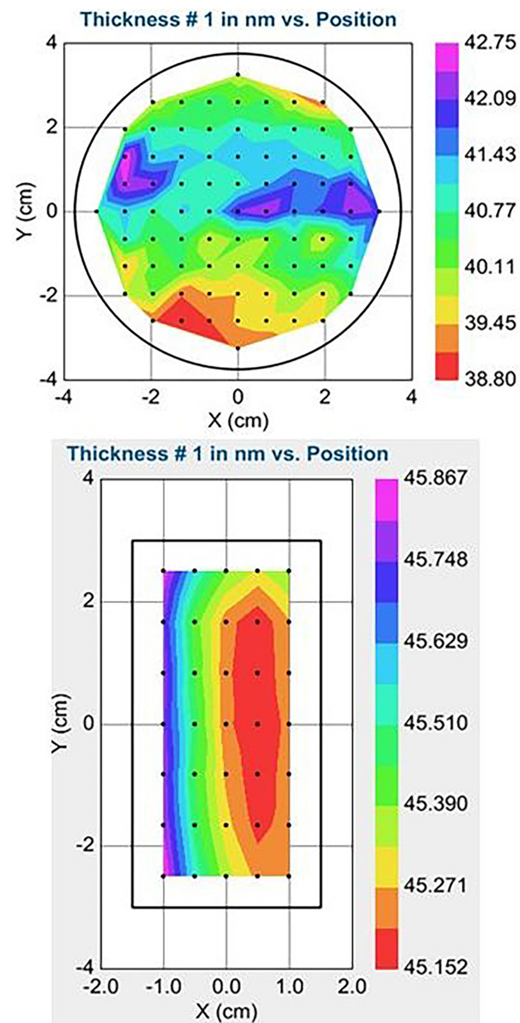

FIG. 7. Examples of the results of VASE measurement of the DLC film thickness for a target thickness of 40 nm on a 3 in. wafer substrate (top) and a target thickness of 45 nm on top of a facet (bottom). Note that the variation in the film thickness across the sample area is less than 10%.

The results of the negative ion yield and angular distribution of the IMAP-Lo DLC conversion surfaces are in agreement with the results obtained for the IBEX-Lo DLC conversion efficiency (Wieser *et al.*, 2007; and Wahlström *et al.*, 2013) even though the film was thinner (46 nm compared to 100 nm) and had a higher surface roughness (3.4 Å compared to ∼1 Å). The production process for DLC conversion surfaces is, thus, well established and provides a DLC charge-conversion film with repeatable parameters.

03 June 2024 15:15:42

© Author(s) 2024

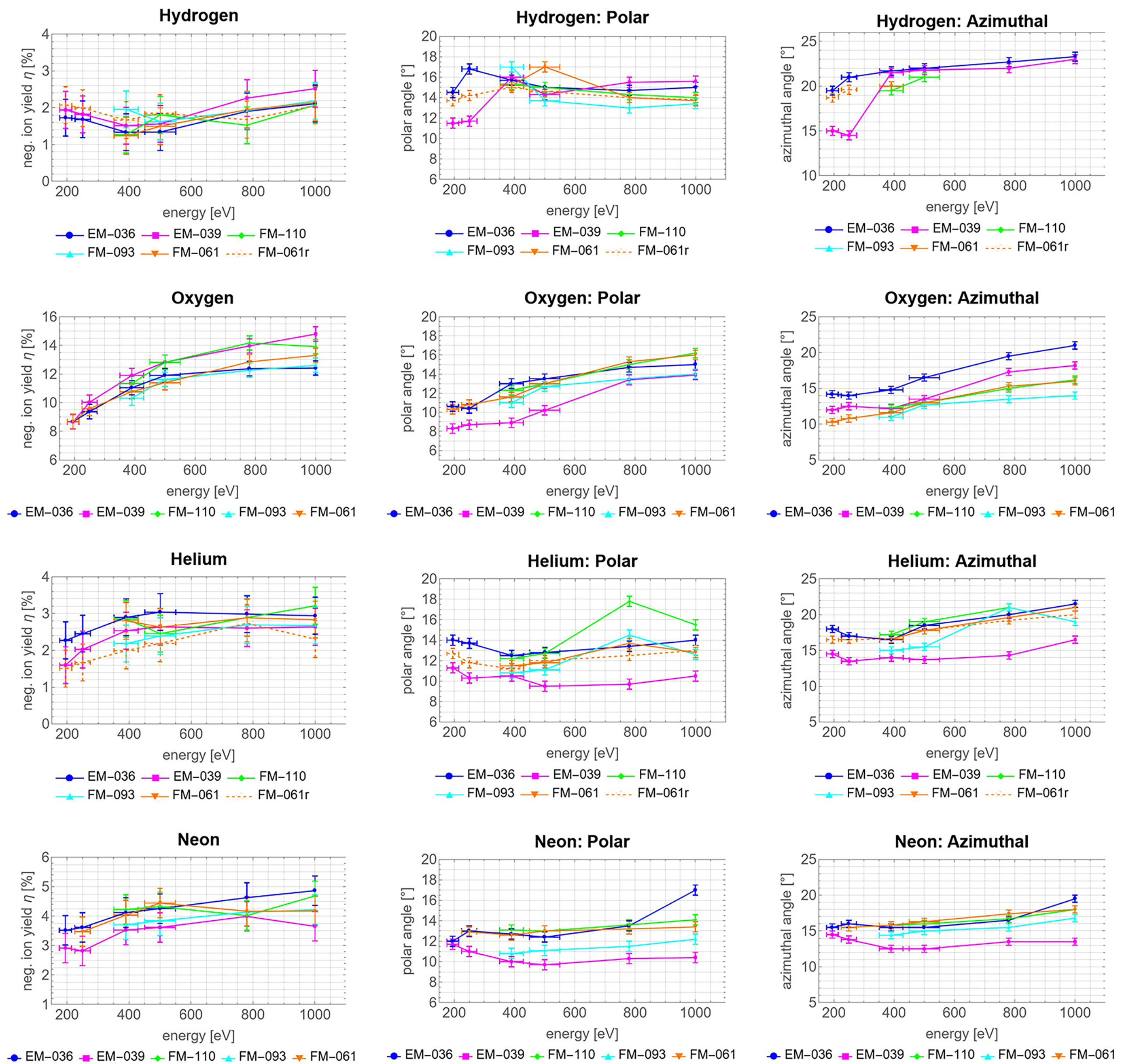

FIG. 8. Negative ion yield (left) and angular scatter in polar (center) and azimuthal (right) directions for the ion beam reflected off the IMAP-Lo DLC conversion surfaces for hydrogen, oxygen, helium, and neon incident beams (from top to bottom) for an energy range between 195 and 1000 eV. EM stands for the engineering model samples, and FM stands for the flight model samples. Some measurements for sample FM-061 were repeated and are illustrated in an orange dashed line (FM-061r).

03 June 2024 15:15:42

IV. SUMMARY

We presented the production process for DLC conversion surfaces used in space instruments for neutral atoms with energies between 10 eV and 2 keV. We described the requirements for substrate selection and substrate preparation for conversion film deposition. We also discussed the coating diagnostic process to determine the coating parameters in a non-invasive way to protect the samples from damage. Our process provides conversion

© Author(s) 2024

surfaces with an ultra-thin coating (46 nm), ultra-smooth surface (3.4 Å), and high conversion efficiency for major species detected in various space environments. We conclude that contamination control throughout the entire process, as well as precision wet and dry cleaning of the substrates before DLC deposition, is crucial for obtaining atomically smooth conversion surfaces. The AFM measurement parameters of the surface roughness should be adapted to the film properties to correctly diagnose the surface smoothness, and the VASE technique can be successfully used in the determination of the coating thickness and uniformity. To make the process more effective, we recommend full automation of the production process to reduce the sample handling and provide a no-touch cleaning, coating, and diagnostic production line.

The DLC conversion surfaces described here are essential elements of the IMAP-Lo instrument. This instrument is one of ten comprising the scientific payload of the IMAP mission scheduled for launch in 2025 for two years of primary operation in the L1 point between the Earth and Sun (McComas *et al.*, 2018).

ACKNOWLEDGMENTS

The authors are thankful to Robert Nemanich for his contribution to the project in the early development phase and to Justin Hrabacek (MPE, Greenville, TX) for his engagement and collaboration in the substrate dicing fulfilling the project requirements. The authors also thank Gabriela Ramirez, Antonia Pevratil, Nate Sennett, Isaac Inverson, Brandon Perez, Sergio Rizo Patron, Paul Wilson, Nicole Lemon, Colin Elder, Joshua Brody, Kenneth Cook, Byron Chapa, Mark Libardoni, Raymond Doty, Ian Karraker, Kenneth Smith, Vicky Poenitzsch, Michela Gargano, Reka Winslow, Dean Hawes, Eberhard Moebius, Harald Mischler, and Adrian Etter for their invaluable contributions and support of the development of the conversion surface coating process for IMAP-Lo at SwRI. This project was supported by the NASA Heliophysics Division, NASA Interstellar Mapping and Acceleration Probe (IMAP) mission, under Contract No. 80MSFC20D0004.

AUTHOR DECLARATIONS

Conflict of Interest

The authors have no conflicts to disclose.

Author Contributions

Justyna M. Sokół: Conceptualization (lead); Data curation (equal); Formal analysis (equal); Investigation (lead); Methodology (equal); Project administration (equal); Supervision (lead); Validation (equal); Visualization (equal); Writing – original draft (lead). **Jianliang Lin:** Formal analysis (equal); Investigation (equal); Methodology (equal); Validation (equal); Writing – original draft (equal); Writing – review & editing (equal). **Stephen A. Fuselier:** Conceptualization (equal); Funding acquisition (equal); Investigation (equal); Resources (equal); Validation (equal); Writing – review & editing (equal). **Travis Eliason:** Data curation (equal); Formal analysis (equal); Investigation (equal); Validation (equal); Writing – original draft (equal); Writing – review & editing (equal). **John E. Gomez:** Data curation (equal); Formal analysis (equal); Investigation (equal); Validation (equal); Writing – original draft (equal); Writing – review & editing (equal). **Benjamin Rodriguez:** Investigation (equal); Resources (equal); Supervision (equal); Validation (equal); Writing – review & editing (equal). **John N Pham:** Investigation (equal); Validation (equal); Writing – original draft (equal); Writing – review & editing (equal). **Clark Schiferl:** Project administration (equal); Resources (equal); Writing – review & editing (equal). **Christopher Rincon:** Investigation (equal). **Cedric Bernier:** Data curation (equal); Formal analysis (equal); Investigation (equal); Validation (equal); Writing – original draft (equal); Writing – review & editing (equal). **Caden Andersson:** Formal analysis (equal); Investigation (equal); Writing – review & editing (equal). **Felicia Mendoza:** Formal analysis (equal); Investigation (equal); Writing – review & editing (equal). **Jonathan Gasser:** Data curation (equal); Formal analysis (equal); Investigation (equal); Validation (equal); Writing – original draft (equal); Writing – review & editing (equal). **Peter Wurz:** Validation (equal); Writing – review & editing (equal). **André Galli:** Validation (equal); Writing – review & editing (equal). **Eric Hertzberg:** Validation (equal). **Nathan A. Schwadron:** Validation (equal).

DATA AVAILABILITY STATEMENTS

The data that support the findings of this study are available from the corresponding author upon reasonable request.

NOMENCLATURE

List of definitions and acronyms used in the presented study.

Acronyms

AFM	Atomic force microscopy
CS	Conversion surface
DI	De-ionized
DLC	Diamond-like carbon
ENAs	Energetic neutral atoms
ESD	Electrostatic discharge
FWHM	Full-width at half maximum
IBEX	Interstellar boundary explorer
ISN	Interstellar neutral (atom)
IPA	Isopropyl alcohol
ILENA	Imager For Low Energetic Neutral Atoms
IMAP	Interstellar Mapping and Acceleration Probe
N/A	Not applicable
PIID	Plasma ion immersion deposition
PP	Polypropylene
SEM	Scanning electron microscopy
SwRI	Southwest Research Institute, San Antonio, TX
UBern	University of Bern, Bern, Switzerland
VASE	Variable angle spectroscopic ellipsometry

Glossary

Angular scatter distribution	Distribution function of the velocity direction of converted and sputtered products
Coating run	A process comprising argon plasma cleaning, DLC deposition, and hydrogen termination

03 June 2024 15:15:42

© Author(s) 2024

Coating set	A set of substrates prepared for the coating process
Conversion surface	Charge-conversion material, e.g., DLC film, deposited on top of a silicon wafer substrate
Converted ions	Ions (positive or negative) created by the charge-exchange process at the conversion surface
Incident beam	Flux of particles hitting the surface at a given angle
Negative ion yield, η	A measured value of the fraction of the converted negative ions to all of the products scattered from the conversion surface
Negative ionization efficiency	Property of the conversion surface to convert a neutral atom or positive ion to a negative ion
Reflected beam	Particles reflecting off the surface comprising scattered and sputtered particles; usually distributed in a 3D cone
Scattered particles	Particles of the primary beam hitting the charge-conversion surface and reflecting off with the charge state changed or not (i.e., a combination of converted and sputtered particles)
Sputtered particles	Secondary particles (ions, atoms), that do not belong to the incident beam, ejected from the material on top of the surface by recoil sputtering, charge state changed or not, e.g., dissociation of the water molecule

REFERENCES

Barabash, S., "The analyzer of space plasmas and energetic atoms (ASPERA-3) for the Mars express mission," Space Sci. Rev. **126**(1–4), 113–164 (2006).

Barabash, S., "The analyser of space plasmas and energetic atoms (ASPERA-4) for the Venus express mission," Planet. Space Sci. **55**(12), 1772–1792 (2007).

Bhandari, N., "Chandrayaan-1: Science goals," J. Earth Syst. Sci. **114**(6), 701–709 (2005).

Bhardwaj, A., "Low energy neutral atom imaging on the moon with the SARA instrument aboard Chandrayaan-1 mission," J. Earth Syst. Sci. **114**(6), 749–760 (2005).

Binnig, G., Quate, C. F., and Gerber, Ch., "Atomic force microscope," Phys. Rev. Lett. **56**(9), 930–933 (1986).

Burch, J. L., "IMAGE mission overview," Space Sci. Rev. **91**, 1–14 (2000).

Funsten, H. O., Allegrini, F., Bochsler, P. *et al.*, "The Interstellar Boundary Explorer High Energy (IBEX-Hi) Neutral Atom Imager," Space Sci. Rev. **146**(1–4), 75–103 (2009).

Fuselier, S. A., "The IBEX-Lo sensor," Space Sci. Rev. **146**(1–4), 117–147 (2009).

Garcia, R. and Perez, R., "Dynamic atomic force microscopy methods,""Dynamic atomic force microscopy methods," Surf. Sci. Rep. **47**(6–8),, 197–301 (2002).

Gasser, J., "Towards better calibration of space instrumentation for measurements of energetic neutral atoms," Ph.D. thesis (Universität Bern, Bern, 2023).

Gasser, J., Föhn, M., Galli, A., Artegiani, E., Romeo, A., and Wurz, P., "Cadmium telluride as a potential conversion surface," J. Appl. Phys. **129**(4), 045303 (2021).

Gasser, J. *et al.*, Rev. Sci. Instrum. **93**, 093302 (2022).

Grasset, O., "Jupiter ICy Moons Explorer (JUICE): An ESA mission to orbit Ganymede and to characterise the Jupiter system," Planet. Space Sci. **78**, 1–21 (2013).

Grigoriev, A., "The neutral particle detector on the Mars and Venus Express missions," Ph.D. thesis (Umeå University, 2007).

Hardij, J. *et al.*, J. Extracell. Vesicles **2**(1), 21045 (2013).

Hsieh, K. C. and Möbius, E., Neutral-Atom Astronomy: Plasma Diagnostics from the Aurora to the Interstellar Medium (World Scientific Publishing Co., 2022).

Johs, B., Woollam, J. A., Herzinger, C. M., Hilfiker, J. N., Synowicki, R. A., and Bungay, C. L., "Overview of variable-angle spectroscopic ellipsometry (VASE). II. Advanced applications," Proc. SPIE **10294,** 1029404 (1999)

Kazama, Y., Barabash, S., Wieser, M., Asamura, K., and Wurz, P., "Development of an LENA instrument for planetary missions by numerical simulations," Planet. Space Sci. **55**(11), 1518–1529 (2007).

Kong, L. G., Zhang, A. B., Tian, Z., Zheng, X. Z., Wang, W. J., Liu, B., Wurz, P., Piazza, D., Etter, A., Su, B., An, Y. Y., Ding, J. J., Li, W. Y., Liu, Y., Li, L., Li, Y. R., Tan, X. and Sun Y. Q., "Mars Ion and Neutral Particle Analyzer (MINPA) for Chinese Mars Exploration Mission (Tianwen-1): Design and ground calibration," Earth Planet. Phys. **4**(4), 333–344 (2020).

Kumara, M., Kumarb, V., Singhc, K., Dubeyd, S., Tiwarie, P. K., Seonga, K. S., and Parka, S. H., Dig. J. Nanomater. Biostruct. **16**(4), 1365–1378 (2012).

McComas, D. J., Allegrini, F., Bochsler, P. *et al.*, Space Sci. Rev. **146**, 11 (2009).

McComas, D. J. *et al.*, Space Sci. Rev. **214,** 116 (2018).

Milillo, A., "The BepiColombo mission: An outstanding tool for investigating the Hermean environment," Planet. Space Sci. **58**(1), 40–60 (2010).

Moore, T. E., "The low-energy neutral atom imager for IMAGE," Space Sci. Rev. **91**, 155–195 (2000).

Neuland, M. B. *et al.*, Appl. Surf. Sci. **313**, 293 (2014).

Oura, K., Lifshits, V. G., Saranin, A. A., Zotov, A. V., and Katayama, M., *Surface Science: An Introduction* (Springer Science & Business Media, 2013).

Pontoni, A., "Development and simulated observations of the Jovian neutrals analyzer," Ph.D. thesis (Universität Bern, Bern, 2022).

Riedo, A., Wahlström, P., Scheer, J. A., Wurz, P., and Tulej, M., "Effect of long duration UV irradiation on diamondlike carbon surfaces in the presence of a hydrocarbon gaseous atmosphere," J. Appl. Phys. **108**(11), 114915 (2010).

Saito, Y., "Scientific objectives and instrumentation of mercury plasma particle experiment (MPPE) onboard MMO," Planet. Space Sci. **58**(1–2), 182–200 (2010).

Simpson, G. J. *et al.*, Langmuir **15**, 1429 (1999).

Scheer, J. A., Wieser, M., Wurz, P., Bochsler, P., Hertzberg, E., Fuselier, S. A., Koeck, F. A., Nemanich, R. J., and Schleberger, M., "Conversion surfaces for neutral particle imaging detectors," Adv. Space Res. **38**(4), 664–671 (2006).

Schwadron, N. A., Möbius, E., McComas, D. J., Bower, J., Bower, E., Bzowski, M., Fuselier, S. A., Heirtzler, D., Kubiak, M. A., Lee, M. A., Rahmanifard, F., Sokół, J. M., Swaczyna, P., and Winslow, R., "Interstellar neutral He parameters from crossing parameter tubes with the interstellar mapping and acceleration probe informed by 10 yr of interstellar boundary explorer observations," Astrophys. J **258**(1), 7 (2022).

Sokół, J. M., Kubiak, M. A., Bzowski, M., Möbius, E., and Schwadron, N. A., "Science opportunities from observations of the interstellar neutral gas with adjustable boresight direction," Astrophys. J **245**(2), 28 (2019).

Sterling, H. F. and Swann, R. C. G., "Chemical vapour deposition promoted by r.f. Discharge," Solid-State Electron. **8**(8), 653–654 (1965). Bibcode:1965SSEle…8..653S. ISSN 0038-1101.

Wahlström, P. *et al.*, J. Appl. Phys. **104**(3), 034503 (2008).

Wahlström, P. *et al.*, "Test facility to study surface-interaction processes for particle detection in space," J. Spacecr. Rockets **50**, 402–410 (2013).

Wan, W. X., Wang, C., Li, C. L *et al.*, "China's first mission to Mars," Nat. Astron. **4**, 721 (2020).

Wieser, M. *et al.*, Nucl. Instrum. Methods Phys. Res., Sect. B **192**, 370 (2002).

03 June 2024 15:15:42

© Author(s) 2024

Wieser, M., Wurz, P., Moebius, E., Fuselier, S. A., Hertzberg, E., and McComas, D. J., "The ion-optical prototype of the low energy neutral atom sensor of the Interstellar Boundary Explorer Mission (IBEX)," Rev. Sci. Instrum. **78**(12), 124502 (2007).

Witte, M., Rosenbauer, H., Keppler, E., Fahr, H., Hemmerich, P., Lauche, H., Loidl, A., and Zwich, R., "The interstellar neutral-gas experiment on ULYSSES," Astron. Astrophys., Suppl. Ser. **92**, 333–348 (1992). https://ui.adsabs.harvard.edu/abs/1992A&AS...92..333W

Woollam, J. A., Johs, B. D., Herzinger, C. M., Hilfiker, J. N., Synowicki, R. A., and Bungay, C. L., "Overview of variable-angle spectroscopic ellipsometry (VASE). II: Basic theory and typical applications," Proc. SPIE **10294,** 1029402 (1999).

Wurz, P., "Detection of energetic neutral particles, The outer heliosphere: Beyond the planets," in *Copernicus Gesellschaft e.V.*, edited by K. Scherer, H. Fichtner, and E. Marsch (Katlenburg-Lindau, Germany, 2000), pp. 251–288.

Wurz, P., Schletti, R., and Aellig, M. R., "Hydrogen and oxygen negative ion production by surface ionization using diamond surfaces," Surf. Sci. **373**(1), 56–66 (1997).

Wurz, P., *et al.*, e-J. Surf. Sci. Nanotechnol. **4**(2006), 394–400 (2006).

Wurz, P., Saul, L., Scheer, J. A., Möbius, E., Kucharek, H., and Fuselier, S. A., "Negative helium generation upon surface scattering: Application in space science," J. Appl. Phys. **103**(5), 054904 (2008).

Ye, P., Sun, Z., Rao, W., and Ming, L., "Mission overview and key technologies of the first Mars probe of China," Sci. China Technol. Sci. **60**(5), 649–657 (2017).

03 June 2024 15:15:42

© Author(s) 2024